THE JOURNAL OF PHYSICAL CHEMISTRY C
A JOURNAL OF THE AMERICAN CHEMICAL SOCIETY

pubs.acs.org/JPCC

Article

Quantum-State-Resolved Scattering of OCS at the Gas−Liquid Interface: Hyperthermal versus Thermal Vibrational Equilibration Dynamics in Polyatomics

Timothy A. Livingston Large and David J. Nesbitt*

Cite This: *J. Phys. Chem. C* 2023, 127, 18586−18597

Read Online

ACCESS | Metrics & More | Article Recommendations

ABSTRACT: Shot-noise-limited direct absorption spectroscopy with a high-resolution quantum cascade laser is used to explore translational-to-rovibrational (T → V, R) energy transfer in hyperthermal collisions ($E_{inc} \approx 21(1)$ kcal/mol) of polyatomic OCS at the gas−liquid interface. Such data provide first evidence for *rovibrational quantum state-dependent* branching into trapping−desorption (TD) and impulsive scattering (IS) pathways for a polyatomic molecule, with unexpected behavior evident due to novel resolution of vibrational degrees of freedom. On the one hand, the rotationally hot IS channel reveals negligible excitation of the OCS bending vibration beyond populations present in the initial supersonic beam ($T_{vib} \approx 220$ K), consistent with a more "spectator" role for polyatomic vibrations ($T_{vib}(IS) \ll T_S$). On the other hand, however, the data sampled at hyperthermal energies exhibit evidence of notably greater vibrational energy transfer, yielding vibrational distributions nearly thermally accommodated with the liquid ($T_{vib}(TD') \approx T_S$), but quite surprisingly only for the rotationally thermalized TD scattering channel at high energy. This is in stark contrast with previous gas−liquid studies of OCS energy transfer *at low* $E_{inc} \approx 2(1)$ kcal/mol, for which complete rotational ($T_{rot}(TD) \approx T_S$) but negligible vibrational ($T_{vib}(TD) \ll T_S$) accommodation occurs, which is in excellent agreement with Landau−Teller−Rapp predictions. Specifically, the results indicate that high energy rovibrational scattering of polyatomics at gas−liquid interfaces involves *nonequilibrium* dynamics more complex than simple branching into "fully thermalized" (TD) and "nonthermalized" (IS) pathways. To help interpret these results, classical molecular dynamics (MD) is explored for OCS rovibrational excitation on a model liquid surface, which indeed confirms that rovibrational energy transfer at the gas−liquid interface is influenced by both (i) surface interaction time and (ii) translational energy dependence of the vibrational excitation rate. The results highlight that the heretofore simply labeled "TD" channel does not necessarily imply complete loss of collisional memory but instead contains incident energy/internal quantum-state-differentiated pathways exhibiting both *equilibrium* and *nonequilibrium* dynamics.

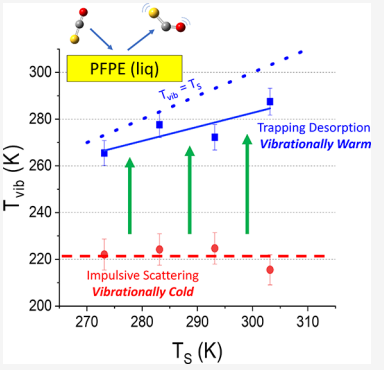

I. INTRODUCTION

Due to high number densities, strong intermolecular interactions, and rapid decay of short-range spatial order, the chemical physics of liquids remains extremely challenging, for which the gas−liquid interfacial region offers additional levels of interest and dynamical complexity. Though such an interface contains only a vanishingly small fraction of a macroscopic liquid sample, this region nevertheless plays a crucial role as "gatekeeper" for gaseous projectiles colliding with the interface in processes varying from (i) thermal accommodation to (ii) quantum-state-resolved molecular solvation and (iii) subsequent chemical reaction in the bulk. Scattering of noble gas supersonic beams at the gas−liquid interface and probing translational energies and angular distributions in the recoiling atoms by time-of-flight (TOF) methods have been extremely informative, as originally pioneered by Fenn and co-workers[1] and elegantly explored by Nathanson et al., Sibener, and others.[2−17] These early studies often (but not always)[17] revealed a surprising simplicity in the collision dynamics. Specifically, TOF distributions for the scattered projectile atoms bifurcate into "trapping−desorption" (TD) and "impulsive scattering" (IS) pathways with a branching fraction α, with the TD channel representing when atoms are trapped long enough to "lose all memory" of initial conditions and eventually desorb. If this TD fraction is exactly unity ($\alpha = 1$), then detailed balance principles rigorously predict the desorbing flux to be in thermal *equilibrium* with the liquid temperature (T_S).[18] In addition, however, these studies also revealed a complementary IS

Received: April 18, 2023
Revised: July 18, 2023
Published: September 7, 2023

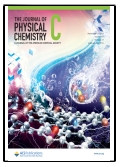

pathway whereby atoms scatter into a nonequilibrium translational distribution and therefore retain memory of the incident collision conditions. By detailed balance considerations, this outgoing IS flux (F_{IS}) must exactly equal the difference between (i) the incident flux under perfect equilibrium conditions (F_{inc}, at $T_{gas} = T_S$) and (ii) the outgoing TD flux (F_{TD}) for molecules that have fully thermally equilibrated (T_S) with the bulk liquid, i.e., $F_{IS} = F_{inc} - F_{TD}$.[18]

The additional challenge in *molecular* scattering at the gas−liquid interface is that such species exhibit internal rovibrational quantum state degrees of freedom beyond those observable via TOF spectroscopies. For *rotations,* however, nature again often offers simplification into two dynamical pathways: (i) a TD channel corresponding to complete *equilibration* (i.e., $T_{rot}(TD) \approx T_S$) and (ii) a complementary IS channel comprising all *nonequilibrium* dynamics. Both TD and IS pathways from hyperthermal scattering experiments have been studied by many techniques, including direct absorption spectroscopy,[4,19−24] time-of-flight mass spectrometry,[2,5,25] and resonance-enhanced multiphoton ionization (REMPI)/velocity map imaging (VMI),[26,27] with studies mostly focused on translational and rotational energy transfer with the surface. The existence of a fully equilibrated TD rotational channel has been additionally confirmed by *temperature-dependent studies* for a number of liquids that exhibit rotational equilibration ($T_{rot}(TD) \approx T_S$) with the interface over a wide range of T_S. Surprisingly, however, these studies often empirically reveal an additional unexpected simplification, specifically that the nonequilibrium IS channel exhibits hot rotational distributions that are well-characterized by a hyperthermal temperature ($T_{rot}(IS) \gg T_S$). Even more surprisingly, for self-assembled monolayer (SAM) surfaces and molecular projectiles (HCl/DCl) accessible via REMPI/VMI methods, there is also quantitative agreement between temperatures measured via final *rotational* (J) and *velocity* vector (v_x, v_z) component distributions in *each* of the TD and IS channels.[26] Indeed, these studies suggest an even simpler physical picture of (i) collisional bifurcation into short-lived IS and longer-lived TD pathways yet (ii) nearly complete equilibration within each of the TD/IS channels between rotational and translational degrees of freedom.[26,27]

Of course, one might expect such simple pictures to break down under sufficient experimental scrutiny. For example, low-energy scattering ($E_{inc} \approx 2(1)$ kcal/mol) of weakly interacting molecules (such as CO or NO) with liquids exhibits interaction times too short to rotationally warm up fully to T_S, i.e., exhibiting "subthermal IS" (STIS) rather than true TD.[21−23,28,29] Simple kinematic models even suggest that the "hot but Boltzmann-like" IS rotational distributions observed for hyperthermal CO or NO ($E_{inc} = 21(1)$ kcal/mol) might not reflect true equilibration but rather J-dependent rainbow scattering smoothed over by, e.g., thermal roughness at the gas−liquid interface.[16] Both the above examples and exceptions highlight the crucial need for theoretical/experimental extension of such models for gas−liquid scattering into new dynamical regimes.

One such area that has remained largely unexplored has been the quantum-state-resolved dynamics of *vibrations* at the gas−liquid interface. Pioneering studies of vibrational energy transfer for diatomics with crystalline solids was achieved by Wodtke and co-workers,[30−32] who reported dramatic differences between NO(v) and CO(v) collisions on conducting versus insulating interfaces. In particular, NO(v) readily deposits multiple quanta of vibrational energy into Au(111) metal surfaces ($\Delta v > 10$), with only perturbative effects ($\Delta v \approx 0, \pm 1$) observed for collisions from insulators such as NaCl. By way of clear contrast, vibrational energy transfer to/from CO(v) was shown by Wodtke and co-workers[32] and Novko and co-workers[33] to be extremely inefficient ($\Delta v \approx 0$) for both metals and insulating materials. Such disparities for NO(v) between metals and insulators have been rationalized by strong coupling with electrons inside the solid. Specifically, NO collisions with metals can energetically access a bound anionic state ($^3\Sigma^+$, NO^-) by electron transfer and become stabilized by Coulomb attraction with the (+) image charge, a pathway unavailable for either insulating surfaces or CO molecular projectiles. As alternatively summarized by Tully and co-workers, NO vibrations in the projectile are always "resonant" with the continuum of electron−hole pair excitations in a conducting metal.[34] This perspective also rationalizes the strong suppression in vibrational relaxation efficiency observed for both NO(v) and CO(v) on insulating materials, as such electron−hole pair excitations become energetically inaccessible.

The present work extends these vibrational excitation ideas further to *polyatomic projectiles*, specifically exploiting high-resolution infrared lasers and molecular beams to study quantum-state-resolved scattering of OCS at hyperthermal energies ($E_{inc} = 21(1)$ kcal/mol) colliding from the gas−liquid interface. OCS is a linear molecule with three internal vibrational degrees of freedom (a CO stretch (ν_1), a doubly degenerate OCS bend (ν_2), and a predominantly CS stretch (ν_3)), with multiple vibrationally excited states accessible at these molecular beam energies.[35] The small rotational constant ($B_{rot} = 0.20286$ cm^{-1}) results in a modest number (∼5−10) of quantum states under jet-cooled conditions and yet an experimentally manageable number (∼300) of rovibrational states at typical beam energies and liquid surface temperatures.[36] By way of context, previous work has shown that vibrational energy transfer in polyatomic OCS scattering from liquid surfaces *at low collision energies* ($E_{inc} \approx 2(1)$ kcal/mol) is extremely inefficient, with the polyatomic vibrations acting as nearly perfect "spectators" in the gas−liquid collision event, in good agreement with Landau−Teller−Rapp modeling of the collision dynamics.[37] This article represents an extension of the previous low-energy studies into the *hyperthermal* ($E_{inc} \approx 21(1)$ kcal/mol) regime, where one might expect such simple adiabatic predictions to begin to fail.

The remainder of this paper is organized as follows. Section II provides experimental details on the polyatomic molecular beam spectrometer, and section III presents results for jet-cooled OCS scattering from perfluoropolyether (PFPE) liquid at high incident energies ($E_{inc} = 21(1)$ kcal/mol) as a function of liquid temperature (T_S). The results recapitulate strong vibrational adiabaticity in the IS dynamics reminiscent of low-energy behavior but now with a completely unexpected sensitivity in the TD channel to T_S. Section IV follows efforts to reproduce these surprising experimental trends with molecular dynamics (MD) trajectory calculations based on *ab initio* scattering potentials. Section V concludes with a summary of key results and directions for further investigation.

II. EXPERIMENTAL SECTION

The gas−liquid scattering laser spectrometer apparatus used in this work for quantum-state-resolved scattering has been described elsewhere[16,28,37,38] and warrants only a brief

https://doi.org/10.1021/acs.jpcc.3c02554
J. Phys. Chem. C 2023, 127, 18586−18597

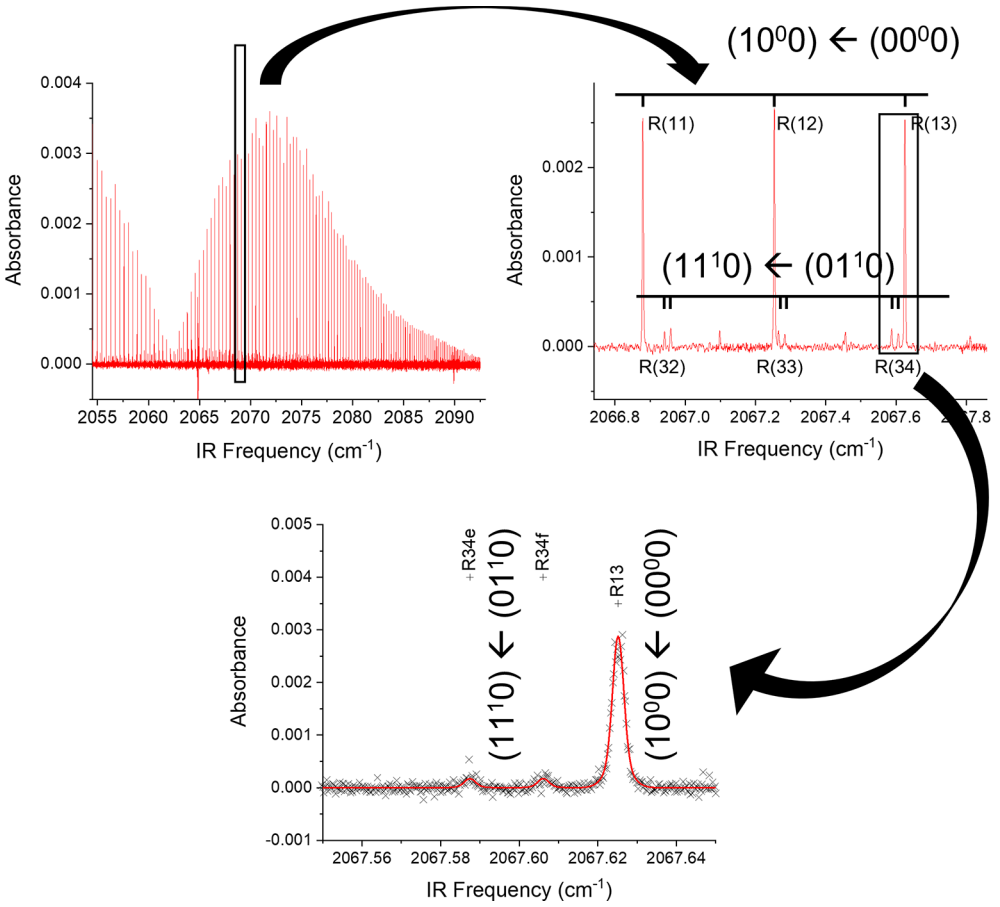

Figure 1. Full sample high-resolution infrared spectrum of OCS scattered from liquid perfluoropolyether (PFPE) at E_{inc} = 21(1) kcal/mol (upper left panel), with blowup regions illustrating progressively more detail in the rovibrationally resolved spectral features. The upper right panel reveals both fundamental $(10^00) \leftarrow (00^00)$ and bending hot band $(11^10) \leftarrow (01^10)$ CO stretch progressions sampling different vibrational manifolds. The lower panel blowup is sufficient to reveal translational Doppler-broadened profiles for each rovibrational transition as well as comparison of experimental data with the high-resolution model fit. Note the order of magnitude decrease in (01^10) vibrational state populations, which explains the absence of any higher-order multiple-quanta excitations detected in the current studies.

overview, with focus on changes relevant to the present study. The light source is an external cavity quantum cascade laser (Daylight Solutions), which can generate ∼300 mW of single-mode infrared light scanned under computer control over the 2000−2200 cm^{-1} spectral window with a sub-Doppler line width of ∼10 MHz. The studies take advantage of cascading frequency measurements for spectral calibration from a traveling Michelson interferometric wavemeter (Bristol 671B) for rough characterization (<0.1 cm^{-1}), with signals transmitted through both an off-axis confocal Fabry−Perot etalon (FSR = 250 MHz, finesse ≈ 20−30) and a room-temperature OCS gas cell (0.5 Torr, 5 cm path length) for precision measurement of absolute and relative frequencies (∼0.001 cm^{-1}) during the actual scan.[39] The internal quantum state (rovibrational) and translational Doppler profiles of the incident and scattered OCS are measured by direct IR laser absorption methods, achieved via subtracting signal and reference beams on matched InSb detectors and with the signal beam executing a 16-fold Harriot cell multipass across the scattering region.[3,19,40] With balanced, fast analog electronics, subtraction of signal and reference beams routinely achieves nearly shot-noise-limited absorbance sensitivities of ∼1 × 10^{-5} in a 10 kHz experimental bandwidth for ∼20 μW laser power on each detector.[16,37]

The scattering measurement system consists of a piezoelectric molecular beam source, a vertical rotating wheel liquid target, and a laser multipass, with the laser propagating perpendicular to the scattering plane formed by the pulse molecular beam axis and the rotating wheel surface normal. The piezoelectric beam source[41] contains 5% OCS in a balance of H_2 expanded through a 500 μm orifice at a stagnation pressure of ∼70 Torr, conditions which optimize signal while still ensuring operation in a OCS nonclustering regime with the signal linearly proportional to the backing pressure. The average molecular beam speed of 1700(70) m/s (measured with a time-of-flight microphone setup) results in an incident OCS collision energy of 21(1) kcal/mol. The molecular beam impinges on the surface 65° from the liquid surface normal with an ∼8 mm diameter collection region centered around the specular scattering angle. Scattered molecules are probed from $\theta \approx -40$ to 75°, with peak collection efficiency around the specular direction ($\theta_{spec} \approx +65°$) and 70% of the OCS molecules detected at $\theta > 45°$. The rotational temperature of the cold molecule beam is $T_{rot} \approx 10$ K, with a much warmer vibrational temperature ($T_{vib} \approx 220(5)$ K) estimated from Boltzmann fits to the (00^00), (01^10), and (00^01) vibrational state populations.

As described in detail elsewhere,[28] the liquid surfaces are prepared according to procedures developed by Lednovich and

https://doi.org/10.1021/acs.jpcc.3c02554
J. Phys. Chem. C 2023, 127, 18586−18597

Fenn,[1] with a rotating ($\omega \approx 0.2$ Hz) bead-blasted stainless steel wheel (12.7 cm diameter) half-submerged in a temperature controlled liquid reservoir and scraped with a stationary razor blade to present a thin (~500 μm), freshly prepared gas–liquid surface to the impinging molecular beam. The liquid reservoir is thermally isolated from the rest of the system by using Teflon spacers, with its temperature stabilized by a two-stage cooling apparatus. The bulk of the cooling/heating is achieved by an ethanol recirculating chiller, which in turn is servoed to a thermistor epoxied to the front of the copper trough.

This study involves three liquids known from previous studies to exhibit differing scattering behavior: (1) perfluorinated polyether (PFPE) (Krytox 1506, $F-[CF(CF_3)-CF_2O)]_{14(avg)}-CF_2CF_3$), (2) squalane (2,6,10,15,19,23-hexamethyltetracosane, $C_{30}H_{62}$), and (3) glycerol (1,2,3-propanetriol, $C_3H_8O_3$).[20,37] All three liquids have low vapor pressures, with the highest (glycerol, 0.2 mTorr) still resulting in mean free collision paths greater than the dimensions of the vacuum chamber. The liquids are degassed under ~1 mTorr vacuum at room temperature for several hours to remove atmospheric gases or at slightly elevated temperatures (~350 K) for the glycerol liquid samples to allow for more complete degassing within a reasonable time frame.

Each experiment consists of sampling 2000 μs long absorption traces for the scattered gas pulse on a single rovibrational transition, with small frequency steps ($\Delta\nu$ = 3–7 MHz) over the appropriate ν_1 CO stretch fundamental and $\nu_1 + \nu_2 \leftarrow \nu_2$, $\nu_1 + \nu_3 \leftarrow \nu_3$ hot band frequency range for OCS (2054.5 to ~2090 cm^{-1}). This complete scan range is broken up into smaller "continuous" step scans (~0.8 cm^{-1}) with a spacing of 0.7 cm^{-1} and thus an approximately 0.1 cm^{-1} overlap to eliminate spectral gaps. Each time trace is converted into absolute absorbance by integrating over the rising edge of the gas pulse (300 μs) and then subtracting an equivalent baseline integration window 400 μs before the start of the signal. Relative frequencies for each scan are obtained by linear interpolation between etalon peak maxima in a Fabry–Perot optical cavity, with absolute frequencies estimated by start/stop frequency measurements from the Bristol wavemeter. These initial frequency estimates are then improved to <0.001 cm^{-1} absolute precision by referencing each scan segment to the HITRAN database.[39]

III. RESULTS AND ANALYSIS

IIIA. Vibrational-State-Resolved OCS Scattering Data.

To combine individual scans and extract quantum-state-resolved column-integrated molecular densities, a global fit to the full scattering spectra is performed,[42] with sample spectral regions displayed in Figure 1. This fit serves two purposes: the first is to stitch each of the individual scans into a global frequency axis, and the second is to permit extraction of scattered molecular populations. The final adjustment to the frequency axis is thus a simple linear transformation, where the global slope and linear offset for each scan are varied to adjust for small (~10 ppb typical) day-to-day changes in the unstabilized etalon free spectral range (FSR) and for any inaccuracies in the calibrations. First of all, the spectral model assumes negligible upper-state population for each spectroscopic transition, which is an excellent approximation for vibrations ~2000 cm^{-1} above the ground state. Second, we assume that the Gaussian transition line shapes arise from a common velocity distribution for each J state, which can be expressed as a linear superposition:

$$A(f_j) = \sum_i S_i(f_j) P_i \tag{1}$$

where $A(f_j)$ is the predicted spectrum and $S_i(f_j)$ is the Doppler transition line shape ($\Delta\nu$ fitted) out of lower state i with column-integrated populations P_i at frequency f_j. The complete list of transitions, transition frequencies, and integrated cross sections in eq 1 was obtained from the HITRAN database,[43] with only transitions for the two predominant isotopomers ($^{16}O^{12}C^{32}S$ (94%) and $^{16}O^{12}C^{34}S$ (4%)) considered. Although the experimental and theoretical spectra contain over 1000 transitions, extraction of the desired lower-state column-integrated densities by least-squares fitting of $A(f_j)$ to eq 1 represents a well-behaved problem in matrix linear algebra.[37]

Sample extracted J- and vibrational-state-dependent populations from such an inversion procedure for collisions of the OCS scattering from PFPE liquid are illustrated in Figure 2,

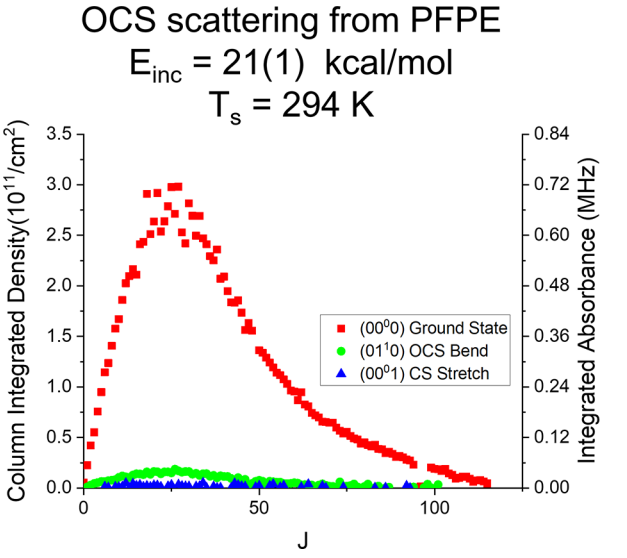

Figure 2. Sample extraction of quantum-state-resolved rovibrational OCS data from the scattering spectra in Figure 1, revealing substantial populations in the ground (00^00), OCS bend (01^10), and CS stretch (00^01) excited lower levels at E_{inc} = 21(1) kcal/mol.

with further parsing of the data (Figure 3) in the form of Boltzmann plots of $\ln[P(J)/(2J+1)]$ versus E_{rot} for the ground (00^00) and ν_2 (01^10) bend excited vibrational states. The dual slope behavior of the logarithmic data in Figure 3 reflect rotational distributions clearly characterized by a two-temperature Boltzmann model, as often observed in hyperthermal scattering experiments.[16,37,44,45] These population fits assume a common Gaussian distribution in the lower-state velocity components, whereas a more flexible and accurate description allows for different Doppler distributions for the TD and IS channels. This model achieves excellent least-squares Doppler fits to the high-resolution spectral scans (e.g., Figure 1), with velocity distributions depending on the TD/IS branching ratios characteristic of each vibrational state manifold. Specifically, transitions out of a given vibrational state are fit to a two-component Gaussian line shape, with TD/IS Doppler widths and branching ratios determined by global fits to the entire spectrum. As used in previous gas–liquid scattering studies, such a translation–rotation model is

https://doi.org/10.1021/acs.jpcc.3c02554
J. Phys. Chem. C 2023, 127, 18586–18597

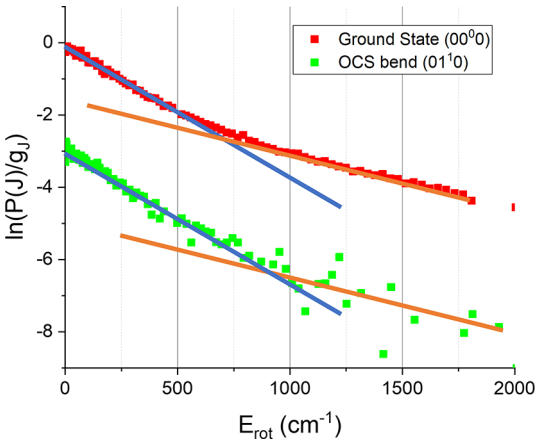

Figure 3. Sample rotational Boltzmann plot for supersonically cooled OCS scattered at E_{inc} = 21(1) kcal/mol from the PFPE gas−liquid interface into the two lower-state vibrations ((00^{0}0) in red, (01^{1}0) in green). Note the clear break evident in each Boltzmann curve, consistent with dual-temperature microscopic branching into trapping desorption (TD′) and impulsive scattering (IS) channels, where we distinguish the high-energy TD channel by the additional prime. Note also that fitted TD′ and IS lines intersect at different rotational energies for different lower-state vibrational manifolds, indicating a shift in the IS/TD′ branching ratio (α) as a function of vibrational excitation.

$$\frac{A(J,f,v_i)}{S_{J,v_i}(2J+1)N} = \alpha_i P_{rot}(J, T_{TDrot}) P_{trans}(f, T_{TDvel}) + (1-\alpha_i) P_{rot}(J, T_{ISrot}) P_{trans}(f, T_{ISvel}) \quad (2)$$

where P_{rot} is a Boltzmann distribution in rotational degrees of freedom, P_{trans} is a Gaussian Maxwell−Boltzmann distribution describing the transverse velocity component for a given vibrational manifold, and α_i is the fractional population in the TD channel scattering into a specific vibrational manifold v_i.

Such modeling, however, does not include coupling between the rotational and vibrational degrees of freedom, which represents an important focus of this work. Indeed, the Boltzmann plots in Figure 3 illustrate that the crossover (i.e., "kink") between the TD and IS distributions depends on the vibrational state, which from eq 2 corresponds to different α_i values. One way to capture such effects is that instead of fitting α_i values for each vibrational state, we choose a single global branching fraction α, with the TD and IS manifolds then characterized by vibrational temperatures T_{vib}(TD′) and T_{vib}(IS), respectively. Such a vibration−rotation-translation model can be written as

$$\frac{A(J,f,v)}{S_{J,v}(2J+1)N} = \alpha P_{rot}(J, T_{rot}(TD')) P_{trans}(f, T_{trans}(TD')) P_{vib}(v, T_{vib}(TD')) + (1-\alpha) P_{rot}(J, T_{rot}(IS)) P_{trans}(f, T_{trans}(IS)) P_{vib}(v, T_{vib}(IS)) \quad (3)$$

where for later purposes we now distinguish the TD scattering channel observed at high versus low E_{inc} by an additional prime (i.e., TD′ vs TD).

The scattering spectral data can be fit to eq 3 by floating six temperatures ($T_{rot/trans/vib}$ for both the TD′ and IS channels), the branching ratio (α), and the overall normalization (N). To reduce parameter correlation, the TD′ rotational and translational temperatures are fixed at the bulk liquid values (T_{rot}(TD′) ≈ T_{trans}(TD′) ≈ T_S), i.e., a rotational/translational equilibrium condition explicitly demonstrated in the previous study,[37] though such a constraint does not change any reported rovibrational temperatures within experimental uncertainties. A sample spectral fit region is illustrated in Figure 1, where the sequential blowup highlights both the dual-temperature Doppler line shapes (e.g., broadening of the Gaussian base) and dramatic differences in signal strengths for transitions arising from (00^{0}0), (01^{1}0), and 00^{0}1) lower-state vibrational manifolds. We note from Figures 1 and 2 that the populations scattered into even these single-quantum excited states of OCS are already small (<7−8%), which makes monitoring multiple-quanta excitation dynamics[46] unfeasible at our current experimental sensitivity and range of T_S.

These hyperthermal quantum-state-resolved energy transfer dynamics have been further augmented by studies on two additional liquids: a "softer" hydrocarbon surface (squalane) and a strongly hydrogen-bonded scattering target (glycerol), with the combined fits results for all four floated temperature degrees of freedom and three liquids are summarized in Figure 4. If we first focus on the nonvibrational results (orange and green bars), the data are in excellent agreement with previous hyperthermal diatomic scattering studies.[16,19,47] Specifically, both translational and rotational temperatures in the IS channel are 200%−300% higher than T_S, with translations significantly hotter than rotations. Similar trends in rotation/translation excitation have been reported for hyperthermal scattering of CO, H/DCl, and CO_2 at $E_{inc} \approx 30\ kT_S$.[16,20,26,28]

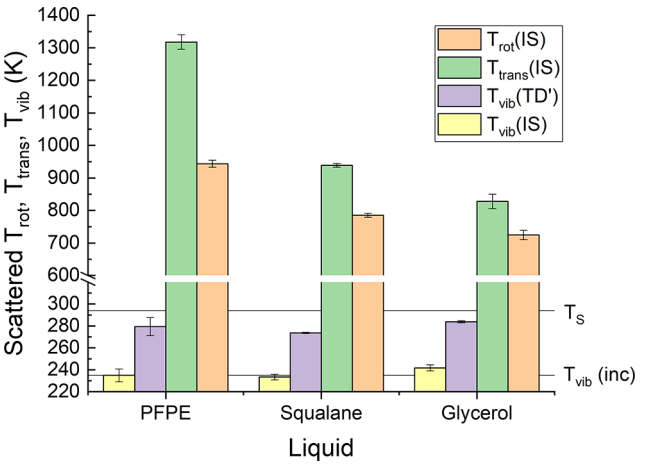

Figure 4. Summary of translational, rotational, and vibrational temperature parameters obtained from least-squares high-resolution fits to the full CO stretch absorption spectrum of OCS scattered at E_{inc} = 21(1) kcal/mol from liquid PFPE.

Of greater dynamical interest is the new information about the polyatomic vibrational degrees of freedom. For the IS channel, the E_{inc} = 21(1) kcal/mol data largely recapitulate previous results at E_{inc} = 2(1) kcal/mol. Specifically, the OCS vibrational temperature (Figure 5, blue squares) neither warms nor cools appreciably from that of the incident molecular beam (T_{vib}(IS) ≪ T_S), implying that little vibrational energy is transferred from either molecule to liquid or liquid to molecule via IS scattering. However, this is in dramatic contrast to what is seen for the TD channel (Figure 5, red circles), where T_{vib}(TD′) "warms up" from the much colder incident beam temperature to nearly that of the liquid surface (T_{vib}(TD′) ≈

https://doi.org/10.1021/acs.jpcc.3c02554
J. Phys. Chem. C 2023, 127, 18586−18597

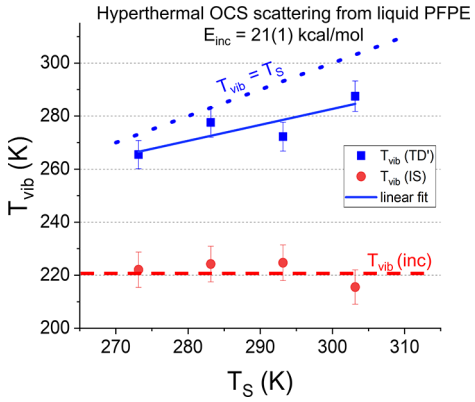

Figure 5. Least-squares-fitted vibrational temperatures for TD′ and IS rotational components obtained from the scattered OCS spectrum as a function of surface temperature at high collision energy E_{inc} = 21(1) kcal/mol. Note that T_{vib} for IS scattering (red line) remains unwarmed from the cold 221 K vibrational temperature of the incident beam, whereas T_{vib} for the TD′ component (blue solid lines) is dramatically warmer (T_{vib}(TD′) ≈ T_S) and clearly sensitive to T_S. This is in stark contrast with low-energy OCS scattering studies,[37] which exhibited fully rotationally thermalized TD scattering ($T_{rot/trans}$(TD) ≈ T_S) **without** vibrational thermalization to the liquid (T_{vib}(TD) ≪ T_S).

T_S). We should stress that the extent of T_{vib}(TD′) warming fully up to the surface temperature (i.e., blue dashed line vs blue solid line in Figure 5) is not the point of crucial comparison. It is instead the striking contrast with the corresponding vibrational behavior in the IS channel (i.e., red dashed line with slope ≈ 0), demonstrating negligible sensitivity to the liquid temperature. One simple physical picture...would be that, at high incident collision energies, the OCS molecule now has the opportunity of thermalizing vibrationally to near surface temperatures, perhaps by virtue of longer surface residence times in the TD′ channel. Of course, the conundrum is that under the *low-energy* collision conditions studied previously, the TD channel showed no corresponding propensity for vibrational equilibration with the liquid.[37] Thus, it must be that access to this novel "vibrational warming" channel both (i) requires hyperthermal incident collision energies and yet (ii) impacts only the fraction of collisions that also rotationally/translationally equilibrate with the liquid (TD′).

To deconstruct these effects in greater detail, hyperthermal quantum-state-resolved OCS scattering from PFPE has also been explored over a range of surface temperatures (T_S), and the dependence of the resulting IS *rotational/translational* temperatures is plotted in Figure 6a. Though the dynamic range of T_S is modest ($\Delta T/T$ ≈ 10%) in absolute terms, the data clearly demonstrate the IS scattering temperatures (T_{rot}(IS), T_{trans}(IS)) to be insensitive to surface temperature. This makes good physical sense at $E_{inc} \gg kT_S$, for which one predicts the outgoing internal energies (and thus scattered "temperatures") to not change significantly with T_S. By way of interesting contrast, however, modest (4−5%) effects on fractional branching (i.e., α) into the TD′ versus IS channel are evident, systematically increasing with surface temperature (Figure 6b). Such α-dependent effects have been reported previously and attributed to a temperature-dependent increase in surface roughness, which in turn can facilitate loss of incident energy and result in a greater propensity for trapping at the gas−liquid interface.[4,14,48]

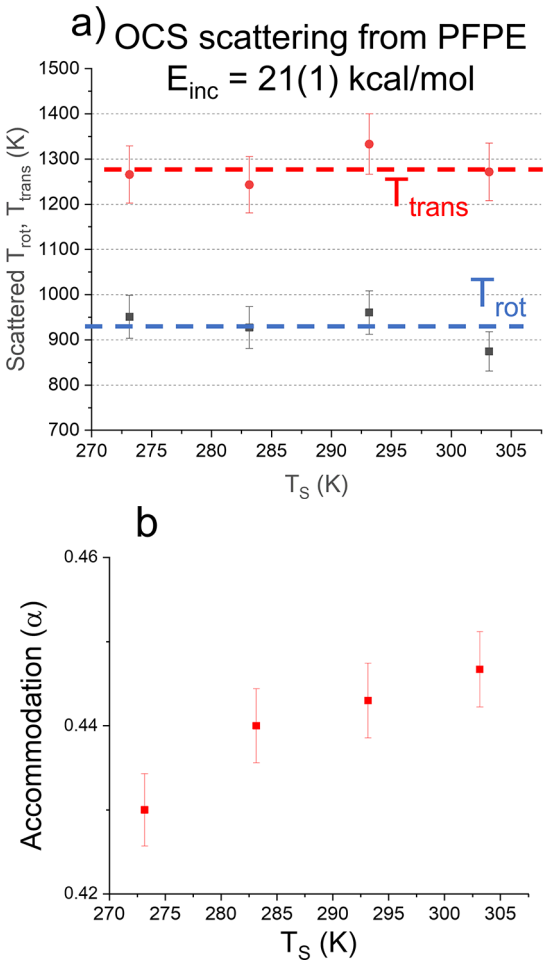

Figure 6. (a) Impulsive scattering (IS) translational and rotational temperature parameters and (b) accommodation coefficients ($\alpha = f_{TD'}/(f_{TD'} + f_{IS})$) obtained from least-squares fit to the scattered OCS spectrum at E_{inc} = 21(1) kcal/mol as a function of surface temperature. Note the modest (4−5%) increase in α yet independence of T_{rot} and T_{trans} on T_S, consistent with previous reports[4,14,48] of increase in surface capillary wave roughness with liquid temperature and decreasing residence times for the IS scattering component at higher collision energies.

However, the most surprising results from these studies are evident in the dependence of the scattered *vibrational* temperatures (T_{vib}(IS) and T_{vib}(TD′)) on T_S. First of all, the IS vibrational temperature (T_{vib}(IS)) behaves as in previous low-energy (E_{inc} = 2(1) kcal/mol) scattering, i.e., not warming from the incident molecular beam temperature (T_{vib} ≈ 222 K), even sampled under these much more hyperthermal collision conditions. Such vibrational adiabaticity would still be consistent with Landau−Teller−Rapp modeling of the T → V collisional dynamics, for which one predicts negligible excitation of the low-frequency OCS bending vibrational modes even at E_{inc} = 21(1) kcal/mol. More surprising, therefore, is the *much greater* sensitivity of the hyperthermal trapping−desorption vibrational component (T_{vib}(TD′)) to T_S, for which the vibrational temperature clearly "warms up" substantially (ΔT ≈ 60 K). We again stress that the crucial comparison in Figure 5 is the contrasting behavior between the linearly increasing solid blue line for T_{vib}(TD′) and the red-dashed line with vanishing slope for T_{vib}(IS). At first glance, this result seems counterintuitive, with vibrational excitation

https://doi.org/10.1021/acs.jpcc.3c02554
J. Phys. Chem. C 2023, 127, 18586−18597

for the TD′ channel *at high energies* behaving similarly to what might have[37] been expected for TD scattering *at low energies*, i.e., complete equilibration with the liquid T_S for all vibrational/rotational/translational degrees of freedom. By way of comparison, the blue-dashed line in Figure 5 represents the limit of full vibrational equilibration ($T_{vib} \approx T_S$), against which the T_{vib}(TD) data (blue points) and linear fit (blue solid line) clearly demonstrate significant vibrational warming from the incident beam (T_{vib}(inc) = 220 K). Although more theoretical analysis will be necessary to deconstruct such *nonequilibrium* quantum-state-resolved excitation dynamics, one simple physical interpretation would be that the TD′ channel accessed via hyperthermal scattering reflects the fortuitous combination of (i) high enough initial collision energy and yet (ii) long enough collisional interaction with the surface to facilitate vibrational equilibration. To set this in proper context, however, it is instructive to remember that any such *nonequilibrium* energy-dependent dynamics in the *vibrational excitation channel* violates the canonical TD paradigm of complete "loss of memory" with respect to incident collision conditions.

IIIB. Theoretical Molecular Dynamics Simulations. To gain further physical insight into this novel TD′ paradigm, we have explored these ideas with molecular dynamics simulations, specifically using the Venus05 platform developed by Hase and co-workers.[37,49,50] In brief, an OCS molecule is selected from a 15 K rotational distribution with $E_{vib} = 0$ and launched at a tunable collision energy (E_{inc} = 1−20 kcal/mol) and incident angle ($\theta = 65°$) toward a thermalized fluorinated SAM (FSAM) surface (T_S) utilizing a full-dimensional FSAM−OCS interaction potential as described previously. This trajectory is propagated until, after having executed at least one sign reversal in the center of mass (COM) velocity, the OCS molecule reaches the initial 25 Å distance from the gas−liquid interface, at which point the interaction potential is negligible ($V \ll kT_S$) and the gas−liquid surface collision is declared complete. One then performs normal-mode analysis in mass-weighted Cartesian coordinates for each of the OCS nuclear positions and momenta to project out and record all vibrational, rotational, and translational energy contributions to the total asymptotic energy.[51]

To help interpret such TD-paradigm-violating quantum-state-resolved experimental dynamics more quantitively, approximately 1000 MD trajectories for this FSAM−OCS potential are calculated at each of several hyperthermal collision energies (E_{inc} = 2, 5, 10, 15, 20, and 50 kcal/mol and T_S = 300 K), with an additional 500 trajectories run at the lowest "subthermal" values (E_{inc} = 0.1 and 0.5 kcal/mol). Sample slices through this much larger data set are displayed in Figure 7a for the resulting rotational energy distributions, which now exhibit only weak signs of dual-temperature-like behavior at the very lowest energies (at $E_{rot} < kT_S$). Indeed, the majority of the OCS molecules scatter in rotational distributions best described by a single temperature T_{rot}, which in turn increases gradually with E_{inc}. To simplify such comparisons and minimize any model-dependent effects, Figure 7b reformulates the theoretical data in terms of an "effective" rotational temperature ($T_{rot} \approx \langle E_{rot}\rangle/k$) as a function of E_{inc}. Above some critical energy ($E_{inc} \approx 5$ kcal/mol), such a plot reveals $\langle E_{rot}\rangle$ to scale approximately linearly with incident collisional energy, with a threshold energy ($E_{thresh} < 5$ kcal/mol) below which the OCS molecules accommodate and desorb into final states rotationally equilibrated with T_S.

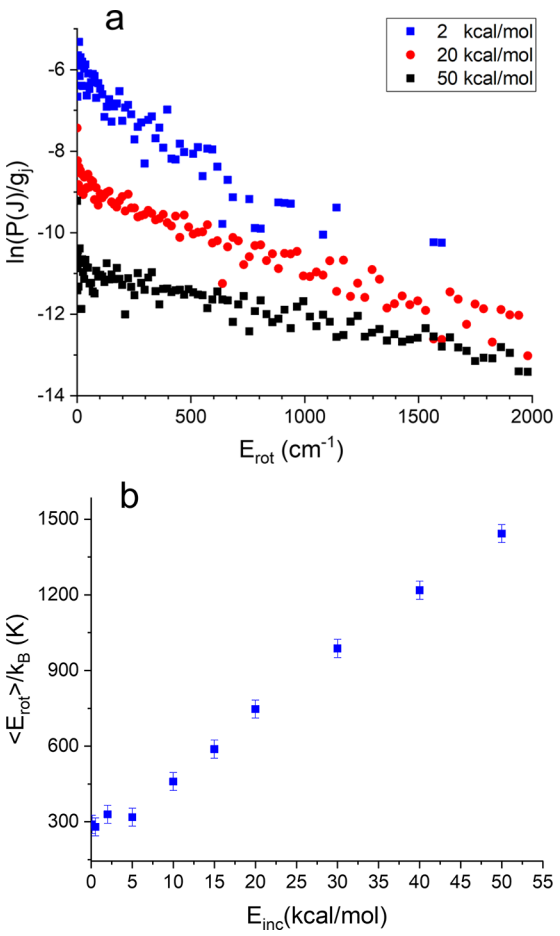

Figure 7. (a) Rotational Boltzmann plot of molecular dynamics (MD) trajectory simulation data, indicating a systematic warming as a function of sample incident collision energy, E_{inc} = 2 (blue), 20 (red), and 50 (black) kcal/mol. There is likely additional TD′/IS structure in the Boltzmann plot, which is not evident due to limited trajectory statistics and why we focus on $\langle E_{rot}\rangle/k$ as the average OCS rotational temperature. (b) Average OCS rotational temperatures ($T_{rot} \approx \langle E_{rot}\rangle/k$) from trajectory calculations vs incident collision energy over 2 orders of magnitude (E_{inc} = 0.5 to 50 kcal/mol) dynamic range.

IIIC. Landau−Teller−Rapp Model Predictions. To understand the more complex vibrational dynamics in these polyatomic MD trajectories, we track both (i) the total energy and (ii) the specific vibrational energies, where mode-specific energies contained in a given polyatomic vibration are calculated from atomic positions and momenta in the asymptotically scattered OCS. Specifically, the OCS molecule is rotated into the Eckart frame, with kinetic and potential energies for each of the three vibrational normal modes (the CO stretch (ν_1), the doubly degenerate bend (ν_2), and the CS stretch (ν_3)) projected out by normal-mode analysis in mass-weighted Cartesian coordinates.[52,53] Sample mode-specific vibrational energy distributions generated at high collision energy (E_{inc} = 20 kcal/mol) are displayed in Figure 8a, where the data for the three vibrations have been displaced for visual clarity. Crudely summarized, vibrational populations in the ν_2 bend manifold look the most "temperature-like" (i.e., exhibit linear semilogarithmic Boltzmann plots), with the ν_1 CO stretch and ν_3 CS vibrations less so and the CO ν_1 mode with a clearly extended high-energy tail.

https://doi.org/10.1021/acs.jpcc.3c02554
J. Phys. Chem. C 2023, 127, 18586−18597

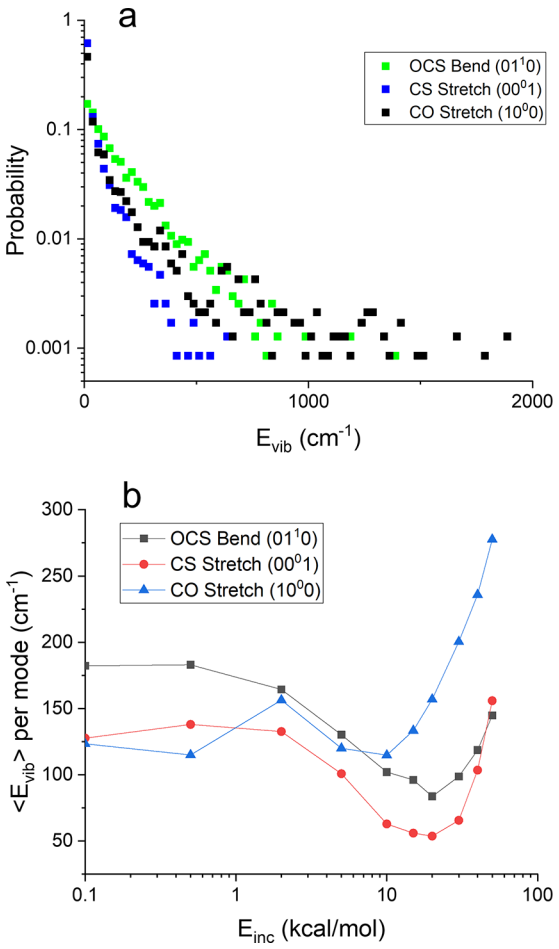

Figure 8. (a) OCS vibrational distributions from MD trajectory calculations scattered (E_{inc} = 20 kcal/mol) into each vibrational mode at T_S = 300 K (kT_S = 208 cm^{-1}). (b) Average energy from MD calculations for the scattered OCS parsed by vibrational mode and as a function of incident collision energy. Note the sharp rise in excitation probability at high E_{inc} and the energy-insensitive plateaus near E_{inc} = 0 (see text for details).

Ideally, one would run sufficient MD trajectories to identify the separate TD′ and IS *rotational* contributions (as in Figure 3), extract *vibrational* temperatures from each of these TD′ and IS rotational channels, repeat as a function of surface temperature T_S, and thereby permit direct comparison with the experimental results in Figure 5. Unfortunately, these vibrational probabilities are quite small, and acquiring sufficient statistics requires several orders of magnitude more trajectories than currently feasible. We can, however, calculate the dependence on incident energy at a single T_S = 300 K. Thus, by way of analogy to the rotational data in Figure 7a, we display in Figure 8b the average OCS scattered vibrational energy per mode $\langle E_{vib}\rangle$ as a function of incident collision energy. It is clear from this figure that the average vibrational energy transfer per mode is low compared with the surface energies $kT_S \approx 300$ cm^{-1}, with indications of a steep growth in efficiency at the very highest collisional energies explored. Furthermore, unlike the experimental data (for which the OCS vibrations are thermally populated and inefficiently cooled in the supersonic expansion), the corresponding MD trajectories start with zero initial vibrational energy, and thus, the final energies observed must arise completely from energy transfer mediated by the surface.

Interestingly, vibrational warming of the OCS molecule exhibits a maximum at both *low* and *high* collision energies, with a minimum energy transfer at E_{inc} of ∼10−20 kcal/mol. At the highest energies, the steep increase in vibrational energy transfer can be rationalized from simple Landau−Teller theory, for which vibrational excitation probability scales as

$$P_{0\to 1} \sim \exp\left(-\frac{2\pi\omega}{\alpha v_0}\right) \tag{4}$$

where ω is the vibrational angular frequency, v_0 is collisional velocity, and α is the logarithmic derivative of the interaction potential evaluated near E_{inc}.[54] Based on numerical estimates of $\alpha \sim 6(1)$ Å^{-1}, one predicts an ∼10-fold increase in average excitation probabilities between 20 and 50 kcal/mol incident energy, in qualitative agreement with these trajectory calculations.[37] In the corresponding low-energy limit, one expects Landau−Teller excitation to be completely negligible and thus requires a different mechanism for vibrational transfer. In a trapping−desorption mechanism, for example, a lowering of E_{inc} would imply less energy available for subsequent molecular *desorption* from the surface, which could yield exponential growth in residence time and probability of subsequent warming to T_S. However, if such a vibrational warming were complete, one would predict equivalent thermalization of all OCS modes at the lowest collision energies, which is not observed (Figure 8b). Instead, the vibrational populations exhibit asymptotically flat behavior at low E_{inc}, with most energy in the lowest-frequency bend ($\langle E_{vib}\rangle \approx 180$ cm^{-1} vs $kT_S \approx 208$ cm^{-1}) and the higher-frequency CO and CS stretch modes lagging by 30%. Although more sophisticated theoretical efforts would be required to confirm these ideas, such a combination of high- and low-energy collision mechanisms nevertheless already captures many trends in the MD trajectory results. For example, a greater thermalization of the lower frequency of the OCS bend versus stretch modes would be consistent with the exponentially slower predictions of eq 4.

IIID. Potential of Mean Force. To interpret the collision energy dependence of the OCS vibrational energy transfer dynamics in even more quantitative detail, we performed statistical mechanical analysis of the MD trajectories. Specifically, we focus on two ancillary studies at low (2 kcal/mol) and high (20 kcal/mol) collision energies with the full phase space coordinates (positions and momenta) of the OCS collider recorded at every 3 fs (10 cycles of the MD propagator). Though such high I/O trajectories are computationally expensive, ∼750 ns long simulations at each collision energy are readily achieved. Most importantly, such trajectories permit calculation of the potential of mean force (POMF) based on methods described previously for low-energy CO scattering.[28] For a nonequilibrium system, the *thermodynamic POMF* is the effective potential at a given coordinate (e.g., distance from the surface, R) averaged over all other degrees of freedom during a series of gas−surface collisions. As a parametric function of R, we can thereby explore how average forces between the projectile and the liquid interface impact vibrational energy transfer dynamics for low (E_{inc} = 2 kcal/mol) and high (E_{inc} = 20 kcal/mol) collision energies. Figure 9 displays the resulting POMF(E_{inc}; R) calculated from MD trajectories at these two values of E_{inc}. One striking difference between these two curves is that the more impulsive high-energy collisions (20 kcal/mol) exhibit a much shallower

https://doi.org/10.1021/acs.jpcc.3c02554
J. Phys. Chem. C 2023, 127, 18586−18597

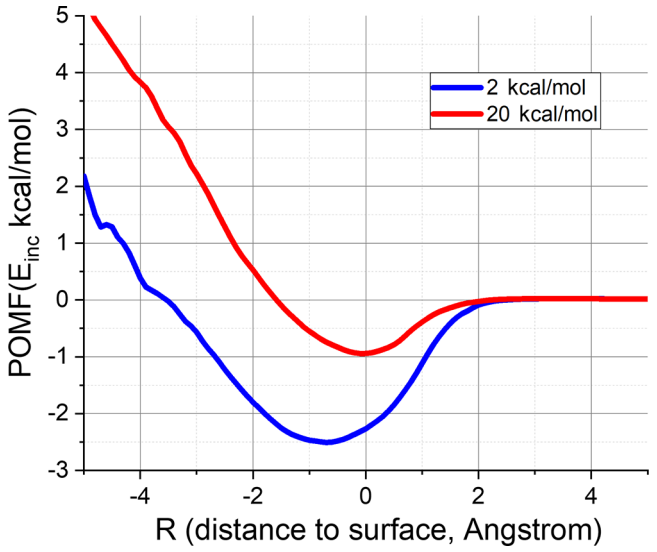

Figure 9. Potential of mean force (POMF) extracted from MD trajectory simulations for high (E_{inc} = 20 kcal/mol) and low (E_{inc} = 2 kcal/mol) collision energies, where R = 0 Å represents the 50% dropoff point in average F atom density from the terminal $-CF_3$ group. Van der Waals contact betweenthe OCS center of mass and the PFPE surface occurs beween $R = -1$ and 0 Å. The plot does not extend to $R < -5$ Å since insufficient trajectories penetrate deeply enough for statistics in that region.

POMF well depth with $R_{eq} \approx 0$ than for low-energy collisions (2 kcal/mol) sampling more deeply into the interface ($R_{eq} < 0$). Furthermore, at the same distance R from the gas−liquid interface, higher collision energies consistently access regions of higher POMF values. Much of this behavior is to be expected since the potential from the gas−liquid interface required to scatter OCS molecules with higher kinetic energies is correspondingly higher. However, the two potentials do exhibit remarkably comparable slopes in the interior region ($\partial V/\partial R \approx -2$ kcal mol^{-1} Å^{-1}), which imply *equivalent repulsive forces* felt by the OCS molecule in both low- and high-energy trajectories *even after molecular penetration into the interface*. Although more work is clearly necessary for validation, this dispersion in POMF shape with energy could reflect a linear combination of trajectories that either (i) thermalize (TD), as captured predominantly in the low-energy POMF, or (ii) promptly reflect (IS) due to strong repulsive interactions between high-energy OCS projectiles and the surface. If so, the energy-dependent shapes in the low- and high-energy POMFs could qualitatively recapitulate the microscopic branching dynamics into what we have experimentally characterized as TD′ and IS channels.

IV. DISCUSSION: VIBRATIONAL BREAKDOWN OF THE TD VERSUS IS PARADIGM

The usual dynamical assumptions for microscopic branching at the gas−liquid interface can be simply summarized as (i) the TD channel corresponds to "complete memory loss" of the initial scattering conditions and (ii) the IS channel comprises all dynamics that is *not* TD scattering. The remarkable validity of this TD/IS branching paradigm has been empirically verified in numerous translational TOF studies[2,10,15,48] and, perhaps more surprisingly, also found to accurately describe translational/rotational degrees of freedom in many quantum-state-resolved diatomic gas−liquid scattering studies.[6,16,24,28,38,55] Previous studies have indeed indicated a breakdown of this TD paradigm, whereby scattering at low E_{inc} does not fully thermalize with the surface in all degrees of freedom, with the TD′ pathway characterized as the "Boltzmann component" (BC)[17,31] or "subthermal impulsive scattering" (STIS) channel.[28] The present polyatomic scattering studies provide the first evidence that this TD′ paradigm breaks down in a new and unexpected way, specifically that OCS *rotational and translational* degrees of freedom thermalize with the surface while the extent of *vibrational* thermalization depends sensitively on both the TD′/IS channel and incident beam energy. As a result, the appealingly simple characterization of TD′ dynamics as a fundamentally *equilibrium* scattering pathway in all internal degrees of freedom is at best incomplete and underestimates how vibrational energy transfer to/from the liquid impacts the scattering event.

Although quantum-state-resolved gas−liquid scattering with polyatomic projectiles will undoubtedly require further theoretical/experimental efforts, we offer the following simple physical picture. The high-energy data suggest and are consistent with microscopic branching between three or more scattering pathways. (1) A rovibrationally cold incident molecule scatters impulsively at high energy from the surface, with the projectile leaving the surface *rotationally and translationally excited* but with insufficient time for vibrational energy exchange to/from the liquid (i.e., the canonical IS channel). (2) Alternatively, rovibrationally cold molecules have sufficient incident kinetic energy to penetrate into the liquid, dissipating sufficient translational energy to become trapped in a deep POMF well and generate sufficiently long residence times to allow *translational, rotational, and near vibrational thermalization* with the liquid (i.e., the proposed TD′ channel). (3) Conversely, in the limit of low incident energy, the projectile is trapped in shallow wells near the surface with high efficiency but interacts superficially with the liquid, desorbing before sufficient collisional interaction time has elapsed for vibrational warming (i.e., the usual TD channel). The key point here is the additional threefold diversity (IS vs TD′ vs TD) in dynamical scattering pathways for polyatomic projectiles, with OCS now demonstrating "vibrational" microscopic branching in the IS channel (i.e., due to strong vs weak interactions with OCS projectile vibrations) while the TD channel remains vibrationally unequilibrated.

We can further test the implications of this more diverse model by inspection of the MD trajectory simulation data. Specifically, Figure 10a reflects a scatter plot of average vibrational energy ($\langle E_{vib} \rangle$) gained asymptotically from the liquid versus duration of the collision trajectory (t_{traj}), corresponding to the time to approach, collide with, and then retreat to ≥25 Å above the interface. This distribution is also binned logarithmically versus t_{traj} in the inset, whose approximate linearity suggests a 1/e average $\langle t_{traj} \rangle \approx 15$ ps and that a large fraction of the trajectories occur in <100 ps with very little transfer of vibrational energy. The key findings are summarized in Figure 10b, which parses the average vibrational warming of the OCS bending mode $\langle E_{bend} \rangle$ as a function of incident collision energy (E_{inc}) into short ($t_{traj} \leq 15$ ps) versus long ($t_{traj} > 15$ ps) bins to allow for best separation of "IS-like" versus "TD′- like" trajectories. Consistent with this simple model, OCS molecules at longer ($t_{traj} > 15$ ps) versus shorter ($t_{traj} < 15$ ps) interaction times indicate much greater differential vibrational thermalization effects at low energies compared with these same differences at high collision

https://doi.org/10.1021/acs.jpcc.3c02554
J. Phys. Chem. C 2023, 127, 18586−18597

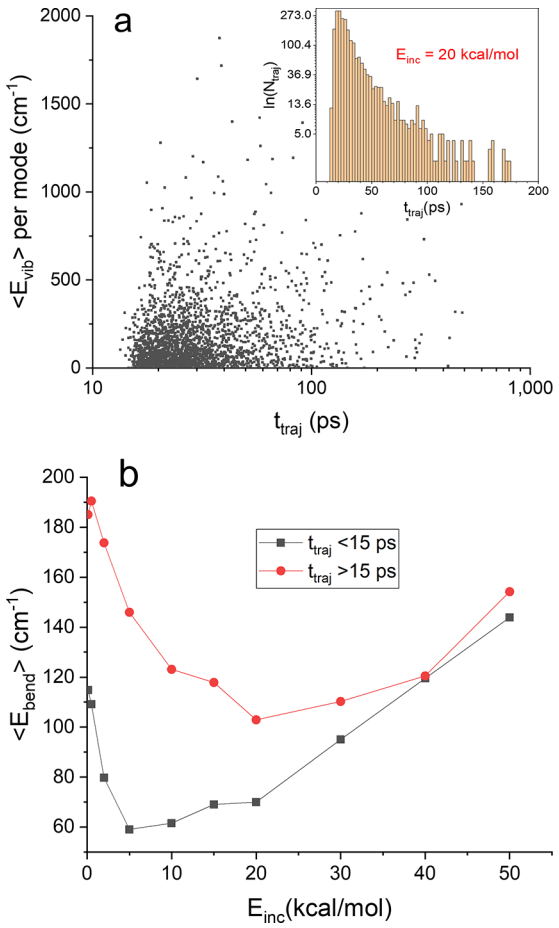

Figure 10. (a) Scatter plot of trajectory duration time (t_{traj}) vs asymptotic average vibrational energy for E_{inc} = 20 kcal/mol. The inset shows the logarithmic histogram of the trajectory durations for this collision energy, with a linear slope corresponding to $\langle t_{traj} \rangle$ = 15 ps. (b) Average vibrational energy in the OCS bending mode summed over all trajectories with $\langle t_{traj} \rangle$ > 15 ps (red) and t_{traj} < 15 ps (black) and plotted as a function of incident OSC collision energy. Note the clear difference between levels of vibrational thermalization ($kT_S \approx$ 208 cm^{-1}) for short-lived ("IS-like") vs long-lived ("TD-like") trajectories and high vs low OCS collision energies.

energies. This physical picture, however, clearly provides only a crude characterization of what are undoubtedly much more diverse and dynamically complex relaxation/excitation phenomena, toward which we hope the current study has provided stimulus for investigation with more sophisticated theoretical methods.

V. SUMMARY AND CONCLUSIONS

Hyperthermal scattering (E_{inc} = 21(1) kcal/mol) of supersonically cooled polyatomic OCS from a series of liquids has been explored as a function of temperature, with high-resolution IR laser spectroscopy permitting quantum-state characterization of the scattered rotational, vibrational, and (perpendicular) translational distributions. Most importantly, polyatomic OCS has low-energy bend and CS stretch vibrational levels that are energetically accessible at these collision energies, which offers first glimpses into the dynamics of "vibrational thermalization" at the gas–liquid interface. The results reveal that OCS rotational/translational degrees of freedom are efficiently excited at high collision energies and well-described by a two-temperature model, corresponding to microscopic branching into trapping–desorption (TD) and impulsive scattering (IS) components as empirically noted for other diatomic projectiles.[16,21,28,29,38]

Interestingly, however, the scattering of OCS with respect to vibrational degrees of freedom does not follow such simple behavior. Specifically unlike low-energy (E_{inc} = 2(1) kcal/mol) studies,[37] for which the TD rotational channel revealed negligible warming of OCS vibrations (T_{vib}(TD) ≪ T_S), microscopic branching at these much higher energies (E_{inc} = 21(1) kcal/mol) preferentially allows OCS vibrations to warm up nearly to the liquid temperature (T_{vib}(TD′) ≈ T_S) in what we designate as the TD′ channel. Conversely, high-energy collisional scattering in the IS channel results in negligible vibrational energy transfer and warming up from cold vibrational temperatures in the incident beam (T_{vib}(IS) ≪ T_S). Simply summarized, polyatomic scattering highlights the *nonequilibrium* diversity in vibrational versus rotational/translational energy transfer pathways at the gas–liquid interface as a function of incident energy.

To interpret this more complex dynamical behavior, classical molecular dynamics has been pursued for OCS polyatomic scattering from a model fluorinated self-assembled hydrocarbon monolayer, with the software allowing deconstruction of final projectile energies into full translation/rotational/vibrational degrees of freedom. The results support a simple physical picture of low-energy collisions (TD channel) resulting in more short-lived gas–liquid interactions and thus relatively inefficient vibrational warming to T_S. Conversely, at high collision energies, the trajectories indicate an exponential increase in vibrational excitation efficiency and are in good agreement with Landau–Teller theoretical expectations. However, additional complexities with respect to OCS vibrational degrees of freedom remain, specifically with the nominal TD or TD′ channels exhibiting either complete (T_{vib}(TD′) ≈ T_S) or negligible (T_{vib}(TD) ≪ T_S) vibrational thermalization in the limit of high and low collision energies, respectively.

One key conclusion from these experiments is that the assumption of the trapping–desorption channel corresponding to the "complete loss of memory" of initial conditions does not capture the full dynamical picture. Specifically, there is a time scale for vibrational energy flow from the liquid to the polyatomic that is finite, incident-energy-dependent, and significant with respect to residence time in the surface well. This naturally results in a more complex picture for energy transfer in polyatomics scattering at the gas–liquid interface but hopefully also a deeper understanding of quantum-state-resolved thermalization and microscopic branching between thermal desorption (TD/TD′) and impulsive scattering (IS) pathways.

AUTHOR INFORMATION

Corresponding Author

David J. Nesbitt − *JILA, National Institute of Standards and Technology and University of Colorado, Boulder, Colorado 80309, United States; Department of Physics and Department of Chemistry, University of Colorado, Boulder, Colorado 80309, United States;* orcid.org/0000-0001-5365-1120; Email: djn@jila.colorado.edu

https://doi.org/10.1021/acs.jpcc.3c02554
J. Phys. Chem. C 2023, 127, 18586−18597

Author

Timothy A. Livingston Large − *JILA, National Institute of Standards and Technology and University of Colorado, Boulder, Colorado 80309, United States; Department of Physics, University of Colorado, Boulder, Colorado 80309, United States*

Complete contact information is available at: https://pubs.acs.org/10.1021/acs.jpcc.3c02554

Notes

The authors declare no competing financial interest.

■ ACKNOWLEDGMENTS

Funding for this work was provided by the National Science Foundation under Grants CHE-1665271/2053117 from the Chemical, Structure, Dynamics and Mechanisms-A Program, with early support for the QCL laser and initial apparatus construction from PHY-1734006 (Physics Frontier Center Program) and Air Force Office of Scientific Research (FA9550-15-1-0090).

■ REFERENCES

(1) Lednovich, S. L.; Fenn, J. B. Absolute evaporation rates for some polar and nonpolar liquids. *AIChE J.* **1977**, *23*, 454−459.

(2) Nathanson, G. M. Molecular beam studies of gas-liquid interfaces. *Annu. Rev. Phys. Chem.* **2004**, *55*, 231−255.

(3) Perkins, B. G., Jr.; Nesbitt, D. J. High resolution Dopplerimetry of correlated angular and quantum state-resolved CO_2 scattering dynamics at the gas-liquid interface. *Phys. Chem. Chem. Phys.* **2010**, *12*, 14294−14308.

(4) Perkins, B. G.; Nesbitt, D. J. Quantum state-resolved CO_2 collisions at the gas-liquid interface: Surface temperature-dependent scattering dynamics. *J. Phys. Chem. B* **2008**, *112*, 507−519.

(5) Faust, J. A.; Nathanson, G. M. Microjets and coated wheels: Versatile tools for exploring collisions and reactions at gas-liquid interfaces. *Chem. Soc. Rev.* **2016**, *45*, 3609−3620.

(6) Tesa-Serrate, M. A.; Smoll, E. J.; Minton, T. K.; McKendrick, K. G. Atomic and molecular collisions at liquid surfaces. *Annu. Rev. Phys. Chem.* **2016**, *67*, 515−540.

(7) Faust, J. A.; Sobyra, T. B.; Nathanson, G. M. Gas-microjet reactive scattering: Collisions of HCl and DCl with cool salty water. *J. Phys. Chem. Lett.* **2016**, *7*, 730−735.

(8) DeZwaan, J. L.; Brastad, S. M.; Nathanson, G. M. The roles of salt concentration and cation charge in collisions of Ar and DCl with salty glycerol solutions of NaI and CaI_2. *J. Phys. Chem. C* **2008**, *112*, 3008−3017.

(9) Chorny, I.; Benjamin, I.; Nathanson, G. M. Scattering, trapping, and ionization of HCl at the surface of liquid glycerol. *J. Phys. Chem. B* **2004**, *108*, 995−1002.

(10) Behr, P.; Morris, J. R.; Antman, M. D.; Ringeisen, B. R.; Splan, J. R.; Nathanson, G. M. Reaction and desorption of HCl and HBr following collisions with supercooled sulfuric acid. *Geophys. Res. Lett.* **2001**, *28*, 1961−1964.

(11) DeZwaan, J. L.; Brastad, S. M.; Nathanson, G. M. Evidence for interfacial $[FDCl]^-$ in collisions between DCl and F^- in KF-glycerol solutions. *J. Phys. Chem. C* **2008**, *112*, 15449−15457.

(12) Morris, J. R.; Behr, P.; Antman, M. D.; Ringeisen, B. R.; Splan, J.; Nathanson, G. M. Molecular beam scattering from supercooled sulfuric acid: Collisions of HCl, HBr, and HNO_3 with 70 wt % D_2SO_4. *J. Phys. Chem. A* **2000**, *104*, 6738−6751.

(13) Ringeisen, B. R.; Muenter, A. H.; Nathanson, G. M. Collisions of DCl with liquid glycerol: Evidence for rapid, near-interfacial D → H exchange and desorption. *J. Phys. Chem. B* **2002**, *106*, 4999−5010.

(14) King, M. E.; Nathanson, G. M.; Hanninglee, M. A.; Minton, T. K. Probing the microscopic corrugation of liquid surfaces with gas-liquid collisions. *Phys. Rev. Lett.* **1993**, *70*, 1026−1029.

(15) Saecker, M. E.; Nathanson, G. M. Collisions of protic and aprotic gases with hydrogen-bonding and hydrocarbon liquids. *J. Chem. Phys.* **1993**, *99*, 7056−7075.

(16) Livingston Large, T. A.; Nesbitt, D. J. Quantum state and doppler-resolved scattering of thermal/hyperthermal DCl at the gas−liquid interface: Support for a simple "lever arm" model of the energy-transfer dynamics. *J. Phys. Chem. C* **2019**, *123*, 3449−3460.

(17) Gibson, K. D.; Isa, N.; Sibener, S. J. Experiments and simulations of hyperthermal xe interacting with an ordered 1-decanethiol/Au(111) monolayer: Penetration followed by high-energy, directed ejection. *J. Phys. Chem. A* **2006**, *110*, 1469−1477.

(18) Tully, J. C. The dynamics of adsorption and desorption. *Surf. Sci.* **1994**, *299*, 667−677.

(19) Perkins, B. G.; Nesbitt, D. J. Stereodynamics at the gas-liquid interface: Orientation and alignment of CO_2 scattered from perfluorinated liquid surfaces. *J. Phys. Chem. A* **2010**, *114*, 1398−1410.

(20) Perkins, B. G.; Nesbitt, D. J. Quantum-state-resolved CO_2 scattering dynamics at the gas-liquid interface: Incident collision energy and liquid dependence. *J. Phys. Chem. B* **2006**, *110*, 17126−17137.

(21) Zutz, A.; Nesbitt, D. J. Quantum state-resolved molecular scattering of $NO(^2\Pi_{1/2})$ at the gas-$[C_nmim][Tf_2N]$ room temperature ionic liquid interface: Dependence on alkyl chain length, collision energy, and temperature. *AIP Adv.* **2016**, *6*, 105207.

(22) Zutz, A.; Nesbitt, D. J. Nonadiabatic spin-orbit excitation dynamics in quantum-state-resolved $NO(^2\Pi_{1/2})$ scattering at the gas-room temperature ionic liquid interface. *J. Phys. Chem. C* **2015**, *119*, 8596−8607.

(23) Ziemkiewicz, M. P.; Zutz, A.; Nesbitt, D. J. Inelastic scattering of radicals at the gas-ionic liquid interface: Probing surface dynamics of Bmim-Cl, Bmim-BF_4, and Bmim-Tf_2N by rovibronic scattering of $NO[^2\Pi_{1/2}(0.5)]$. *J. Phys. Chem. C* **2012**, *116*, 14284−14294.

(24) Lane, P. D.; Moncrieff, K. E.; Greaves, S. J.; McKendrick, K. G.; Costen, M. L. Inelastic scattering of CN radicals at the gas−liquid interface probed by frequency-modulated absorption spectroscopy. *J. Phys. Chem. C* **2020**, *124*, 16439−16448.

(25) Muenter, A. H.; DeZwaan, J. L.; Nathanson, G. M. Collisions of DCl with pure and salty glycerol: Enhancement of interfacial D → H exchange by dissolved NaI. *J. Phys. Chem. B* **2006**, *110*, 4881−4891.

(26) Hoffman, C. H.; Nesbitt, D. J. Quantum state resolved 3D velocity map imaging of surface scattered molecules: Incident energy effects in HCl plus self-assembled monolayer collisions. *J. Phys. Chem. C* **2016**, *120*, 16687−16698.

(27) Roscioli, J. R.; Bell, D. J.; Nelson, D. J.; Nesbitt, D. J. State-resolved velocity map imaging of surface-scattered molecular flux. *Phys. Chem. Chem. Phys.* **2012**, *14*, 4070−4080.

(28) Livingston Large, T. A.; Nesbitt, D. J. Low-energy CO scattering at the gas-liquid interface: Experimental/theoretical evidence for a novel subthermal impulsive scattering (STIS) channel. *J. Phys. Chem. C* **2020**, *124*, 28006−28017.

(29) Zutz, A.; Peterson, K. A.; Nesbitt, D. J. Nonadiabatic dynamics at the gas-molten metal interface: State-to-state resolved scattering of NO from hot gallium (600−1000 K). *J. Phys. Chem. C* **2021**, *125*, 341−353.

(30) Wagner, R. J. V.; Kruger, B. C.; Park, G. B.; Wallrabe, M.; Wodtke, A. M.; Schafer, T. Electron transfer mediates vibrational relaxation of CO in collisions with Ag(111). *Phys. Chem. Chem. Phys.* **2019**, *21*, 1650−1655.

(31) Steinsiek, C.; Shirhatti, P. R.; Geweke, J.; Lau, J. A.; Altschäffel, J.; Kandratsenka, A.; Bartels, C.; Wodtke, A. M. Translational inelasticity of NO and CO in scattering from ultrathin metallic films of Ag/Au(111). *J. Phys. Chem. C* **2018**, *122*, 18942−18948.

(32) Shirhatti, P. R.; Rahinov, I.; Golibrzuch, K.; Werdecker, J.; Geweke, J.; Altschaffel, J.; Kumar, S.; Auerbach, D. J.; Bartels, C.; Wodtke, A. M. Observation of the adsorption and desorption of vibrationally excited molecules on a metal surface. *Nat. Chem.* **2018**, *10*, 592−598.

(33) Loncaric, I.; Alducin, M.; Juaristi, J. I.; Novko, D. CO stretch vibration lives long on Au(111). *J. Phys. Chem. Lett.* **2019**, *10*, 1043−1047.
(34) Shenvi, N.; Roy, S.; Tully, J. C. Nonadiabatic dynamics at metal surfaces: Independent-electron surface hopping. *J. Chem. Phys.* **2009**, *130*, 174107.
(35) Davies, P. R.; Orville-Thomas, W. J. Infrared band intensities and bond polarities: Part I. Bond moment constants in CO_2, OCS, CS_2, CSe_2 and SCSe. *J. Mol. Struct.* **1969**, *4*, 163−177.
(36) Herzberg, G. *Molecular Spectra and Molecular Structure, Volume III: Electronic Spectra and Electronic Structure of Polyatomic Molecules*; Van Nostrand Reinhold: New York, 1966.
(37) Livingston Large, T. A.; Nesbitt, D. J. State-resolved studies of OCS scattering at the gas−liquid interface: Tests of Landau—Teller/Rapp theory for rotational vs vibrational energy transfer. *J. Phys. Chem. C* **2021**, *125*, 22786−22796.
(38) Gisler, A. W.; Nesbitt, D. J. On probing ions at the gas-liquid interface by quantum state-resolved molecular beam scattering: The curious incident of the cation in the night time. *Faraday Discuss.* **2012**, *157*, 297−305.
(39) Rothman, L. S.; et al. The Hitran database - 1986 edition. *Appl. Opt.* **1987**, *26*, 4058−4097.
(40) Perkins, B. G.; Nesbitt, D. J. Toward three-dimensional quantum state-resolved collision dynamics at the gas-liquid interface: Theoretical investigation of incident angle. *J. Phys. Chem. A* **2009**, *113*, 4613−4625.
(41) Proch, D.; Trickl, T. A high-intensity multi-purpose piezoelectric pulsed molecular-beam source. *Rev. Sci. Instrum.* **1989**, *60*, 713−716.
(42) Ryazanov, M.; Nesbitt, D. J. Quantum-state-resolved studies of aqueous evaporation dynamics: NO ejection from a liquid water microjet. *J. Chem. Phys.* **2019**, *150*, 044201.
(43) Rothman, L. S.; Gordon, I. E. The HITRAN molecular database. *AIP Conf. Proc.* **2013**, *1545*, 223−231.
(44) Nogueira, J. J.; Vazquez, S. A.; Mazyar, O. A.; Hase, W. L.; Perkins, B. G.; Nesbitt, D. J.; Martinez-Nunez, E. Dynamics of CO_2 scattering off a perfluorinated self-assembled monolayer. Influence of the incident collision energy, mass effects, and use of different surface models. *J. Phys. Chem. A* **2009**, *113*, 3850−3865.
(45) Perkins, B. G.; Nesbitt, D. J. Stereodynamics in state-resolved scattering at the gas-liquid interface. *Proc. Natl. Acad. Sci. U. S. A.* **2008**, *105*, 12684−12689.
(46) Kay, B. D.; Raymond, T. D.; Coltrin, M. E. Observation of direct multiquantum vibrational excitation in gas-surface scattering: NH_3 on Au(111). *Phys. Rev. Lett.* **1987**, *59*, 2792−2794.
(47) Perkins, B. G.; Nesbitt, D. J. Quantum-state-resolved CO_2 scattering dynamics at the gas-liquid interface: Dependence on incident angle. *J. Phys. Chem. A* **2007**, *111*, 7420−7430.
(48) King, M. E.; Fiehrer, K. M.; Nathanson, G. M.; Minton, T. K. Effects of thermal roughening on the angular distributions of trapping and scattering in gas-liquid collisions. *J. Phys. Chem. A* **1997**, *101*, 6556−6561.
(49) Hase, W.; Duchovic, R.; Hu, X.; Komornicki, A.; Lim, K.; Lu, D.; Peslherbe, G.; Swamy, K.; Linde, S. V.; Wang, H. Venus96, a general chemical dynamics computer program. *Quant. Chem. Prog. Exch.* **1983**, *3*, 453.
(50) Martinez-Nunez, E.; Rahaman, A.; Hase, W. L. Chemical dynamics simulations of CO_2 scattering off a fluorinated self-assembled monolayer surface. *J. Phys. Chem. C* **2007**, *111*, 354−364.
(51) Wilson, E. B., Jr.; Decius, J. C.; Cross, P. C. *Molecular Vibrations: The Theory of Infrared and Raman Vibrational Spectra*; McGraw-Hill, 1955.
(52) Louck, J. D.; Galbraith, H. W. Eckart vectors, Eckart frames, and polyatomic molecules. *Rev. Mod. Phys.* **1976**, *48*, 69−106.
(53) Eckart, C. Some studies concerning rotating axes and polyatomic molecules. *Phys. Rev.* **1935**, *47*, 552−558.
(54) Rapp, D.; Sharp, T. E. Vibrational energy transfer in molecular collisions involving large transition probabilities. *J. Chem. Phys.* **1963**, *38*, 2641−2648.
(55) Bagot, P. A. J.; Waring, C.; Costen, M. L.; McKendrick, K. G. Dynamics of inelastic scattering of OH radicals from reactive and inert liquid surfaces. *J. Phys. Chem. C* **2008**, *112*, 10868−10877.

https://doi.org/10.1021/acs.jpcc.3c02554
J. Phys. Chem. C 2023, 127, 18586−18597